

# PERMAFROST STABILITY AND LAND SURFACE TEMPERATURE DISTRIBUTION STUDY USING MULTI-SOURCE REMOTE SENSING DATA IN THE QINGHAI-TIBET PLATEAU

Peng Zhang, Yan Chen, Yunping Chen

School of Automation Engineering, University of Electronic Science and Technology of China,  
Chengdu 611731, China

## ABSTRACT

This paper discusses the temperature factors leading to permafrost instability, and explains the causes of permafrost instability from the perspective of land surface temperature (LST). First, the land surface deformation of the typical permafrost area in some period is extracted by the using the dual-track differential interferometry (D-InSAR) technique with Sentinel-1A single look complex(SLC) data. Next, the annual average LST and LST range are calculated using the spatio-temporal interpolation algorithm for MYD11A2 products. Comparing the distribution of land surface deformation and LST, findings show that permafrost regions with lower average annual LST and larger annual temperature range are more unstable and more prone to surface deformation. This research can contribute to unveiling the process where LST affects the freezing and thawing of permafrost.

**Index Terms**— permafrost, deformation, D-InSAR, land surface temperature

## 1. INTRODUCTION

The change of LST causes the mutual transformation of ice and water in the active layer of permafrost, which may lead to large-scale ground deformation in QTP, and severely damage the regional infrastructure.

Now, the existing research mainly uses the dual-track differential interferometry technique or long-time series differential interferometry to monitor the surface deformation value or deformation rate, and determine the stability of frozen soil according to the deformation results, but the cause of frozen soil deformation is still not fully explained. Therefore, it is very necessary to determine the relationship between permafrost stability and LST and to explore the LST characteristics of unstable permafrost.

At present, numerous researchers use MODIS datas to determine the spatiotemporal distribution of LST[1, 2, 3]. However, due to the occlusion of clouds, there are a large number of missing values in MODIS LST data. And the spatiotemporal interpolation algorithm is currently the most commonly

used method to fill in the missing values in MODIS products. When monitoring the stability of frozen soil,differential interferometric synthetic aperture radar (D-InSAR) is widely used because it can effectively monitor the surface deformation of long-term and large areas[4, 5, 6].

Therefore, in order to determine the relationship between permafrost stability and LST, and to clarify the LST characteristics of unstable permafrost, this paper uses the dual-track differential interference technique to extract the typical permafrost region over a period of time from the Sentinel-1A data, and employs time-space interpolation algorithm to fill in the missing values of MYD11A2 products for consecutive years, and then the dynamic changes of LST in the typical area are monitored. By comparing the results of surface deformation and surface temperature, this paper analyzes the relationship between permafrost stability and surface temperature, and explores the temperature factors that cause permafrost surface deformation.

## 2. METHODOLOGY

### 2.1. MYD11A2 data processing

The 8-day synthetic LST data MYD11A2 with 1km spatial resolution is selected in this paper. As shown in figure 1, we first extracted the irradiance brightness layer and quality control parameter layer of MYD11A2 products for many consecutive years, and determined the pixels occluded by clouds according to the quality control parameters, and then employed the spatiotemporal interpolation algorithm to fill the vacancy values of these points, where the spatial interpolation window is 3\*3.

Then, in order to obtain the LST with physical significance, we applied formulas 1-2, where  $DN$  is the value recorded in MYD11A2 product, the value of  $scale\_factor$  and  $Offset$  is respectively 0.02 and 0, and  $T1$  and  $T2$  respectively represent the converted LST in Kelvin and in Celsius, to convert the irradiation brightness into the real LST. Finally, the converted temperature array is reprojected into WGS84 coordinate system, and the annual average LST and temperature range result in GeoTIFF format is quickly

yanchen@uestc.edu.cn

obtained after mosaicing, and clipping.

$$T1 = \text{scale factor} \times DN + \text{offset} \quad (1)$$

$$T2 = T1 - 273.15 \quad (2)$$

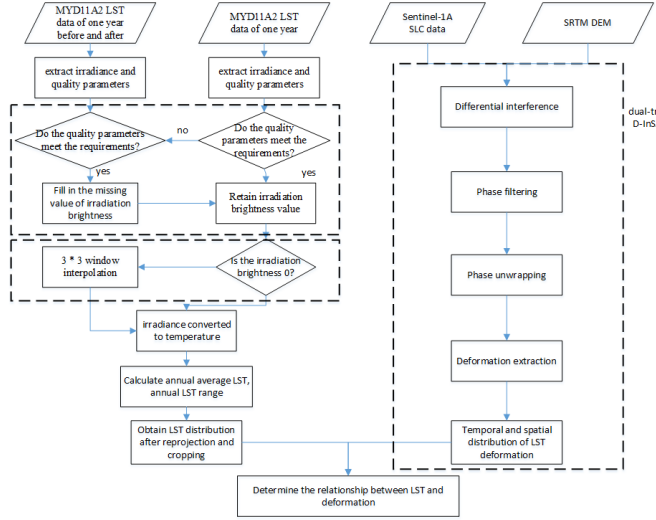


**Fig. 1:** Multi-source data processing flow diagram

## 2.2. D-InSAR processing flow

Shown as table 1, The two Sentinel-1A single look complex (SLC) datas are applied to monitor the surface deformation, and the images dated May 13, 2018 and June 18, 2018 are used as the master and slave images of this paper respectively.

**Table 1:** Information of data used

	Acq.Date	swath	polarization	pass
Master	20180513	IW2	VV	Ascending
Slave	20180618	IW2	VV	Ascending

Moreover, the 90m SRTM DEM data released by NASA is used as the external DEM data to eliminate the influence of topographic factors in the interferometric phase diagram.

As shown in the figure 1 , we employed the dual-track D-InSAR technique with the SRTMDEM data and the precision orbit data, to extract the surface deformation of the above-mentioned two Sentinel-1A SLC datas. And the D-InSAR process is as follows:

(1) interferogram acquisition: By calculating the space-time baseline, the quality of the interference pairs was evaluated after image pre-filtering and image registration. And the terrain phase for differential interference processing was simulated with assistance of the DEM data.

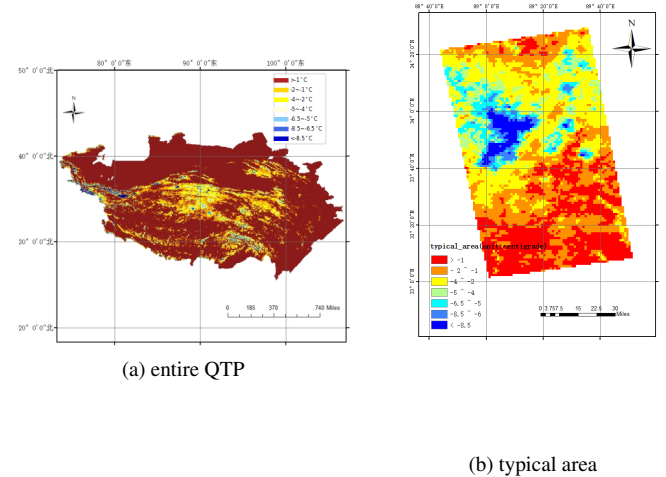


**Fig. 2:** Annual average LST distribution of entire QTP and typical area

(2) interference phase filtering: There is often a lot of phase noise in the original interferogram, which affects subsequent works, so filteing is an inevitable task.

(3) phase unwrapping: The minimum spanning tree method was applied to unwrap the wrapped phase.

(4) extracting deformation: The spatial distribution of deformation was extracted successfully after orbit refining, geocoding.

## 3. RESULTS AND ANALYSIS

### 3.1. LST distribution results

From figure 2a which is the result of the annual average LST distribution in the entire QTP by using MYD11A2 and shp data[7], we can find the temperature in most parts of the QTP are above  $-1^{\circ}\text{C}$ . In order to correctly embody the relationship between surface deformation and temperature distribution, we selected a typical area that contains multiple temperature types at the same time, as shown in Figure 2b. By comparing the composition proportion of the above two as shown table 2, we knew "low-temperature" like  $-8.5 \sim -5^{\circ}\text{C}$  in typical area had been significantly increased, and the proportion of each temperature area is relatively balanced. Which is helpful to analyze the relationship between unstable frozen soil and surface temperature

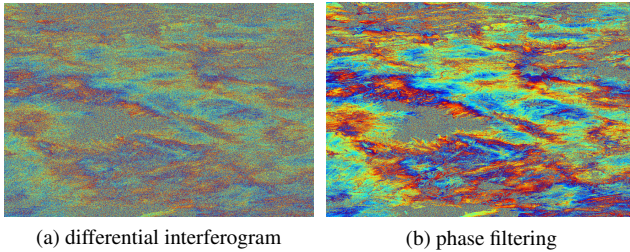
### 3.2. Deformation results in typical area

The differential interferogram is shown in figure 3a, it can be seen that most parts of typical area have obvious interference fringes, which shows that the results of surface deformation extracted from typical area are relatively reliable; figure 3b

**Table 2:** Proportion of each type of temperature distribution

	entire QTP	typical area
>-1	78.3%	23.6%
-2~-1	10.7%	27.8%
-4~-2	6.4%	27.2%
-5~-4	1.7%	9.4%
-6.5~-5	1.3%	6.3%
-8.5~-6.5	0.8%	2.9%
<-8.5	0.8%	2.8%

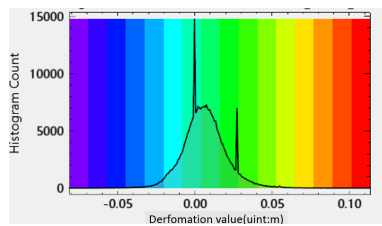
shows fringes are more clearly visible after removing the flat ground effect and filtering. The above results embody good interference effects, which lays a good foundation for further deformation extraction.



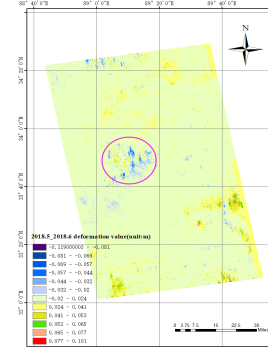
**Fig. 3:** D-InSAR results in typical area

Figure 4 shows the statistical analysis results of surface deformation values in typical area, and it illustrates the deformation is mainly weak deformation of  $-3cm \sim 3cm$  in typical area, although there are also areas with deformation of more than  $10cm$ , but its proportion is extremely low.

Figure 5 represent the distribution results of surface deformation. From the area delineated in figures 5, we found that compared with other areas, the proportion of severe land surface deformation in this area is significantly higher, and the surface deformation is mainly manifested as vertical surface subsidence. That's probably because the sampling time of the master and slave images is May and June respectively, which coincides with the warming of the climate and the increasing of the LST. And The LST changes make the ice contained in the soil of the delineated region be converted to water, re-



**Fig. 4:** Statistics results of deformation



**Fig. 5:** Land surface deformation distribution

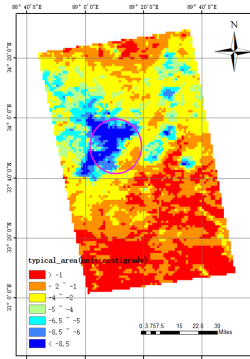


**Fig. 6:** Annual average LST distribution

sulting in an increase in soil moisture content, which causes subsidence.

### 3.3. Comparative analysis of deformation and LST distribution

Figures 6 and 7 represent the distribution results of annual average LST and annual temperature range respectively.

Comparing the delineated region with other ones in Figure 5, 6, and 7, we found that the permafrost regions with severe land surface deformation have relatively lower annual average LST and larger annual temperature range. The lower the annual average LST, the easier the water in the active layer freezes in the cold season; simultaneously, the higher the annual average LST range, the easier the frozen ice is melted into water. The mutual transformation of ice and water causes the "soil body shrinkage" and "soil body expansion", which in turn causes a large surface deformation. Either the higher annual average LST cannot easily cause water to freeze or the lower annual average temperature difference can rarely melt ice, the conversion between ice and water will occur in other areas, which will not generate great fluctuation.

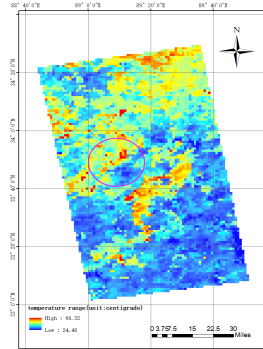


**Fig. 7:** Annual temperature range distribution

#### 4. CONCLUSION

This paper discussed the temperature factors leading to frozen soil instability, and explained the cause of permafrost instability from the perspective of LST.

We first obtained the spatial distribution of the annual average LST and the annual LST range after filling the missing values in the MYD11A2 LST data by using spatio-temporal interpolation algorithm. Next, the SLC data of Sentinel-1A were processed by the dual-orbit D-InSAR technique, and the land surface deformation results of the typical area were extracted. Finally, we compared the distribution of land surface deformation and LST. Findings show that permafrost regions with lower average annual LST and larger annual temperature range are more unstable and more prone to surface deformation. The lower annual average LST will easily freeze the water of active layer in the cold season; meanwhile, the higher annual average LST range will easily melt ice to water. The interconversion between ice and water causes the shrinkage and expansion of the soil, which deforms permafrost surface.

#### 5. FUNDING

This work is supported by the Advance Research Project of Civil space Technology.

#### 6. ACKNOWLEDGMENT

Thanks for the RDS software provided by Xidian University.

#### 7. REFERENCES

- [1] Yuan Qi, Shiwei Li, Youhua Ran, Hongwei Wang, and Dongliang Luo, “Mapping frozen ground in the qilian mountains in 2004–2019 using google earth engine cloud computing,” *Remote Sensing*, vol. 13, no. 1, pp. 149, 2021.
- [2] G. D. Cheng and S. L. Wang, “On the zonation of high-altitude permafrost in china,” *Journal of Glaciology and Geocryology*, 1982.
- [3] Chen Yiyang Fan Zhengui Liu Xiuguo HUANG Bowen, GAO Ruixiang, “Multi-scale monitoring of permafrost in qinghai-tibet plateau using multi-source rs images,” *Safety and Environmental Engineering*, vol. 27, no. 4, pp. 7, 2020.
- [4] Sai Wang, Bing Xu, Wei Shan, Jiancun Shi, Zhiwei Li, and Guangcai Feng, “Monitoring the degradation of island permafrost using time-series insar technique: a case study of heihe, china,” *Sensors*, vol. 19, no. 6, pp. 1364, 2019.
- [5] Z. Zhang, M. Wang, Z. Wu, and X. Liu, “Permafrost deformation monitoring along the qinghai-tibet plateau engineering corridor using insar observations with multi-sensor sar datasets from 1997–2018,” *Sensors (Basel, Switzerland)*, vol. 19, no. 23, 2019.
- [6] Jingyi Chen, Yue Wu, Michael O’Connor, M Bayani Cardenas, Kevin Schaefer, Roger Michaelides, and George Kling, “Active layer freeze-thaw and water storage dynamics in permafrost environments inferred from insar,” *Remote Sensing of Environment*, vol. 248, pp. 112007, 2020.
- [7] Y Du, “Prefecture-level administrative units boundary of qinghai-tibet plateau (2015),” 03 2019.